Journal of Information Analytics, 1(1), 59-72

Journal of Information Analytics

Submit 13.06.2025
Revision 01.07.2025
Accept 01.07.2025
Publish 02.07.2025

Research Article

Open Access

Forecasting Lip Landmark Movements Using Time Series Models

Gözde Nergiz[1], Faruk Serin[2],

[1] Department of Computer Tecnology, Adana Alparslan Turkes Science and Technology University, Adana, Türkiye

[2]Department of Computer Engineering, Mersin University, Mersin, Türkiye

Abstract

This study examines the predictability of time series data derived from lip movements during speech using traditional statistical methods. The dataset was generated from a publicly available video, where x and y coordinates of 40 lip landmarks were extracted for each frame using Google's MediaPipe Face Mesh technology. Comprising a total of 3,242 frames and 80 time series, the dataset was analyzed by applying ARIMA and SARIMA models with various parameter combinations. The lowest Mean Absolute Percentage Error (MAPE) achieved was 0.0994 for the ARIMA model and 0.1331 for the SARIMA model. The most successful parameter combinations for the ARIMA model were typically p=5, d=0, q=1, while for the SARIMA model, the parameters p=1, d=0, q=3, P=0, D=0, Q=1, s=25 demonstrated the best performance.

Keywords Lip movement analysis, MediaPipe face mesh, time series forecasting, ARIMA, SARIMA

Citation: Nergiz, G., & Serin, F. (2025). Forecasting Lip Landmark Movements Using Time Series Models. *Journal of Information Analytics*, 1(1), 59-72.

Corresponding Author: Gözde Nergiz gnergiz@atu.edu.tr

1. Introduction

Humans rely on words to convey emotions and thoughts; however, facial expressions form the core of communication. These expressions, reflecting an individual's thought processes, emotions, and experiences, reveal their unique identity (Ekman, 2003). As social beings, humans employ not only verbal communication but also nonverbal elements such as gestures, facial expressions, and body language (Mast, 2007). The human face is the primary domain where these nonverbal communication elements are most prominently observed.

The face is an integrated structure composed of various subcomponents (eyes, eyebrows, nose, cheeks, and mouth). Among these, the mouth and its surrounding area serve as a central region for both speech production and the vivid expression of emotions. In particular, the lips are key elements that visually enhance the intensity and sincerity of expressions. This rich expressive capacity has laid the foundation for the development of modern facial recognition and tracking systems. With technological advancements, applications based on facial and lip analysis are increasingly integrated into daily life. Examples include facial recognition systems in smartphones, automatic tagging features on social media platforms, driver fatigue detection systems, and security applications. In healthcare, these technologies are utilized to enhance eye contact abilities in individuals with autism spectrum disorder, measure consumer reactions in marketing research, and support augmented reality applications. Given the significance of the human face, many new technologies and studies are actively being pursued. One prominent framework for researchers is the MediaPipe Face Mesh application (Lugaresi et al., 2019). The Face Mesh application is frequently preferred across various domains for its ability to automatically detect and track faces in images or videos (Adhikari et al., 2025; Aripin & Setiawan, 2024; Balaji & Sujatha, 2025; Jakhete & Kulkarni, 2024). Comparative studies have demonstrated its superiority over other methods. For instance, Jakhete and Kulkarni (2024) conducted a comprehensive study on emotion recognition through facial expressions, comparing various methods and datasets. They found that the MediaPipe Face Mesh model, capable of detecting 468 3D facial landmarks in real time, outperformed models like DLIB and OpenPose in terms of accuracy and speed. These technologies are employed in converting speech to text for individuals with hearing impairments, ensuring dubbing synchronization in film and video content, and detecting speech content remotely in forensic science. However, a key challenge in facial analysis is the temporary occlusion of specific facial regions, particularly the lips. Occlusion by hands, hair, or other objects can lead to missing or corrupted movement data (W. Zhang et al., 2023). The human face is characterized by relatively stable positions and sizes of facial components, largely unaffected by environmental factors, which impose strong structural constraints. This is a critical aspect often overlooked by current methods when addressing occluded landmarks (Li et al., 2024). Time series analysis methods have shown promising results in addressing such challenges. Time series analysis is a statistical approach used to examine patterns, trends, and variations in temporally observed data (Shumway & Stoffer, 2025). It is widely applied in fields such as finance (Lu & Xu, 2024; Sui et al., 2024), healthcare (Kong et al., 2024), energy (Gulay et al., 2024), and meteorology (Mishra et al., 2024; Ansari & Alam, 2024).

In this study, the human face in videos is detected using Face Mesh technology, with a focus on the lip region. The x and y coordinates of 40 distinct lip landmarks (resulting in 80-dimensional data) identified through Face Mesh are treated as time series across the video duration. The primary objective of the research is to apply ARIMA and SARIMA methods with different parameter combinations to these coordinate movements, compare the resulting MAPE values, and determine the most optimal forecasting model. The study's findings will contribute to predicting missing or corrupted lip coordinates in cases of temporary occlusion, ensuring the continuity of facial movement analysis. The second section of this study presents a literature review. The third section details the proposed methodology. The fourth section evaluates the findings under the results and discussion section. The final section provides the conclusions.

2. Literature Review

Time series forecasting models can be categorized as univariate and multivariate. Univariate models include AR (Ding et al., 2010), MA (Tsay, 2005), ARMA (Brockwell & Davis, 2016), and ARIMA (Box et al., 2015), while SARIMA (Rosychuk et al., 2016) is prominent for seasonal data, and SARIMAX (Elamin & Fukushige, 2018) is used when exogenous variables are incorporated. For multivariate data, models such as VAR (Zivot & Wang, 2006), VARMA (Tsay, 2013), and VARMAX (Casals et al., 2012) are preferred. For short-term forecasting, methods like SES (X. Zhang et al., 2020) and Holt-Winters (Jiang et al., 2020) offer effective solutions. Various time series models have been employed for forecasting. ARIMA models, characterized by three parameters (p, d, q), are widely applied across domains such as the furniture industry (Yucesan et al., 2018), healthcare (Kadri et al., 2014; Wei et al., 2016; Xu et al., 2016), finance (Zhang et al., 2016), energy (Yuan et al., 2016; Cadenas et al., 2016), food industry (Tripathi et al., 2014), transportation (Mete et al., 2022; Serin et al., 2021), aquaculture (Siddique et al., 2025), climate (Wahyudi & Febriani, 2024). Variants such as vector-ARIMA (Mai et al., 2015), ARMA (Aboagye-Sarfo et al., 2015), SARIMA (Butler et al., 2016; Rosychuk et al., 2016), and MSARIMA (Aroua & Abdul-Nour, 2015) are also frequently utilized by researchers.

Siddique et al. (2025) analyzed air temperature and precipitation data from 2011–2022 in Mymensingh, Bangladesh, using ARIMA models to forecast trends for 2023–2030. Their aim was to predict the impact of climate variables on aquaculture and provide data-driven insights for planning. Data sourced from NASA was validated using Bangladesh Meteorological Department records. The optimal models were ARIMA (2,1,2) for temperature and ARIMA (3,0,2) for precipitation, selected based on statistical metrics such as BIC, RMSE, and MAPE, supported by ACF and PACF graphs. The forecasts indicate a significant temperature increase and precipitation decrease in Mymensingh in the coming years.

Kong et al. (2024) aimed to predict missing values in healthcare data in a time-aware manner. They used Truncated SVD to compress data, reducing redundancy and noise, followed by ARIMA for missing value prediction. Their approach improved accuracy by considering temporal dimensions and capturing essential data patterns, with experiments on the WISDM dataset demonstrating its effectiveness and efficiency.

Wahyudi and Febriani (2024) compared SARIMA and SARIMAX models to predict particulate organic carbon (POC) levels in Indonesia's Sunda Shelf waters using MODIS data from 2002–2022. The models were SARIMA (3,1,3) x (2,0,0,60) and SARIMAX (3,1,3) x (2,0,0,60), with SARIMAX incorporating exogenous variables like sea surface temperature, chlorophyll-a, and salinity. Although SARIMAX had a lower AIC, validation metrics (MAPE, RMSE, correlation coefficient) showed SARIMA's superior performance. Forecasts suggest POC levels will fluctuate seasonally between 108.3–135.9 mg/m^3 from 2022–2030, peaking during the northwest monsoon season.

Kumar et al. (2024) compared Holt-Winters Exponential Smoothing (HWES) and ARIMA models to enhance demand forecasting and dynamic pricing strategies. Tested on real-world data, the models were evaluated for reducing lost sales and optimizing revenue under uncertain market conditions. Their dynamic pricing model, designed for limited sales seasons, also analyzed lost sales patterns. The findings indicate ARIMA's superior performance over HWES in volatile market conditions.

3. Material and Method

Dataset

The dataset used in this study was created from a publicly available YouTube video, with its characteristics detailed in Table 1, utilizing MediaPipe Face Mesh technology (Lugaresi et al., 2019).

Table 1. Basic Information About the Video Used for the Dataset

	Video File Info
Duration	129.68 saniye (~2 dakika 10 saniye)
Frame Rate	25 fps
Total Frame Count	3242

MediaPipe operates in real time, detecting 468 three-dimensional (3D) landmarks on a face. To precisely track lip movements during speech, specific lip landmarks defined by MediaPipe were selected. These landmarks were divided into two groups: the outer lip contour and the inner lip contour, each comprising 20 points. The x and y coordinates of each lip landmark were extracted, forming a dataset with 3,242 rows (corresponding to the total number of video frames) and 83 columns (including id, time, frame, and x and y coordinate values for the 40 landmarks).

ARIMA and SARIMA Models

The AR(p) and MA(q) models applied to forecasting are represented as in Equations (1) and (2), respectively (Yule, 1926; Wold, 1938).

$$Y_t = \sum_{i=1}^{p} a_i \, Y_{t-i} + \varepsilon_t \tag{1}$$

$$Y_t = \varepsilon_t + \sum_{j=1}^{q} b_j \, \varepsilon_{t-j} \tag{2}$$

where a_i are non-seasonal AR parameters, ε_t is zero mean Gaussian noise and b_j are non-seasonal MA parameters.

The ARMA (p, q) model combines p autoregressive terms and q moving average terms, as shown in Equation (3):

$$Y_t = c + a_1 Y_{t-1} + \cdots + a_p Y_{t-p} + \varepsilon_t + b_1 \varepsilon_{t-1} + \cdots + b_q \varepsilon_{t-q} \tag{3}$$

In cases of non-stationary data, differencing is required to achieve stationarity, as in the ARIMA model (Box et al., 2015).

Performance Measurements

The forecasting results were evaluated using the Mean Absolute Percentage Error (MAPE), as defined in Equation (4).

$$MAPE = \left(\frac{1}{n}\sum_{t=1}^{n} \frac{|Y_t - \hat{Y}_t|}{Y_t}\right) * 100 \tag{4}$$

4. Experimental Results

In this study, the ARIMA method was applied with different combinations to each of the 80 time series (40 x-coordinates and 40 y-coordinates) derived from the coordinates of 40 distinct lip landmarks. The combinations were determined by setting the hyperparameter ranges for p, d, and q as 0–9, 0–1, and 0–3, respectively, resulting in 80 different combinations per series, totaling 6,400 evaluations.

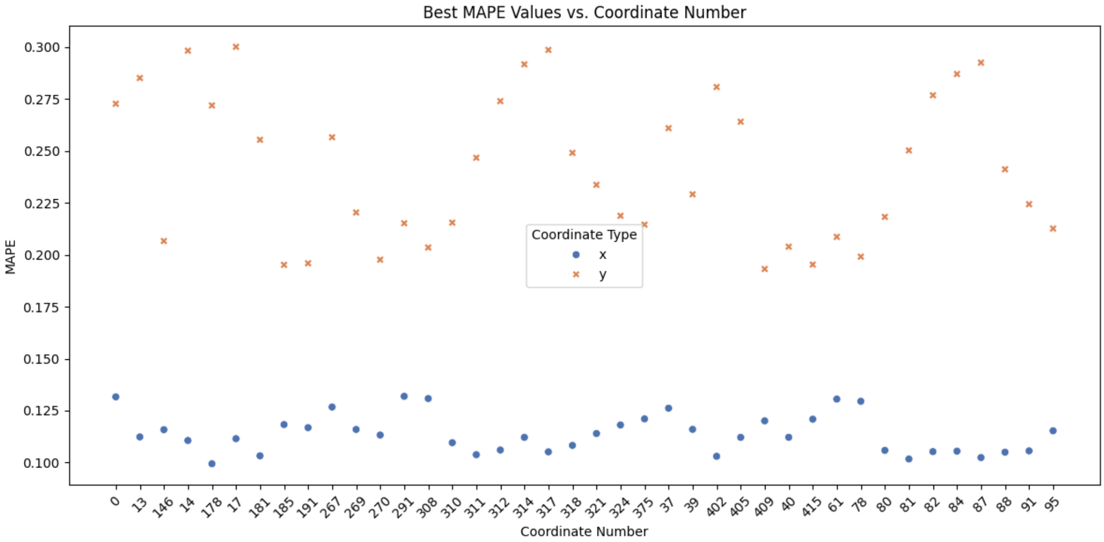

Figure 1. Best MAPE Value for Each Series

Figure 1 displays the best MAPE values for each time series. In the figure, "x" markers (orange) represent the values obtained from the time series of y-coordinates of lip landmarks, while dot markers (blue) represent those from x-coordinates. The x-coordinates (blue) are generally concentrated in the 0.10–0.15 MAPE range, while y-coordinates (orange) are scattered in the 0.20–0.30 range. This suggests that the coordinate type (x or y) is a determining factor in the obtained values.

Table 2. MAPE Statistics by Coordinate Type

Coord. Type	Min	Max	Mean	Median
x	0.10	0.13	0.11	0.11
y	0.19	0.30	0.24	0.24

Table 2 presents the basic statistics obtained by considering the best MAPE values for x and y coordinates. The MAPE average for x-coordinates is 0.113807, with a median of 0.112231, while for y-coordinates, these values are 0.24 and 0.24, respectively. The minimum and maximum values also show that y-coordinates are distributed over a wider range (0.19–0.30) compared to x-coordinates, suggesting greater variation in y-series and thus greater difficulty in prediction.

Table 3. Top 10% of Coordinates with the Lowest MAPE Values and ARIMA Parameter Values

Coordinate	p value	d value	q value	MAPE Score
178_x	5	0	1	0.0994
81_x	5	0	1	0.1017
87_x	5	0	1	0.1024
402_x	5	0	3	0.1030
181_x	9	0	1	0.1032
311_x	3	0	2	0.1038
88_x	5	0	1	0.1050
317_x	6	0	3	0.1051

* MAPE values were rounded to four decimal places to enhance numerical clarity across coordinates.

Table 3 lists the p, d, q values used in the ARIMA method and the corresponding MAPE values for the top 10% of coordinate series with the lowest MAPE values. The first row indicates that for the time series of the x-coordinate of lip landmark 178, applying the ARIMA method with p=5, d=0, and q=1 resulted in a MAPE value of 0.0994.

Table 4. Top 10% of Coordinates with the Highest MAPE Values and ARIMA Parameter Values

Coordinate	p value	d value	q value	MAPE Score
17_y	7	0	2	0.3002
317_y	1	0	3	0.2987
14_y	1	0	3	0.2983
87_y	1	0	3	0.2925
314_y	2	0	3	0.2917
84_y	7	0	2	0.2871
13_y	9	0	1	0.2851
402_y	2	0	3	0.2808

* MAPE values were rounded to four decimal places to enhance numerical clarity across coordinates.

Table 4 shows the highest MAPE values (the top 10% of the 8-coordinate series), ranging from 0.3002 for 17_y to 0.2808 for 402_y. All series in the table consist of y-coordinates of the landmarks. The ARIMA parameters are generally observed to be p=1 or p=2, q=3. This indicates that the modeling challenges for y-coordinates are exacerbated with certain parameter combinations.

Table 5. Top 5 Most Successful ARIMA Parameter Combinations

Count	p value	d value	q value
8	5	0	1
7	7	0	2
6	6	0	1
6	8	0	3
6	4	0	2

Table 5 presents the top five ARIMA parameter combinations based on the frequency of their use in achieving the best MAPE values for the 80 different series. The table shows that the combination p=5, d=0, q=1, used 8 times, ranks first. Additionally, the fact that the d value is 0 in the combinations listed in the table suggests that differencing is generally unnecessary.

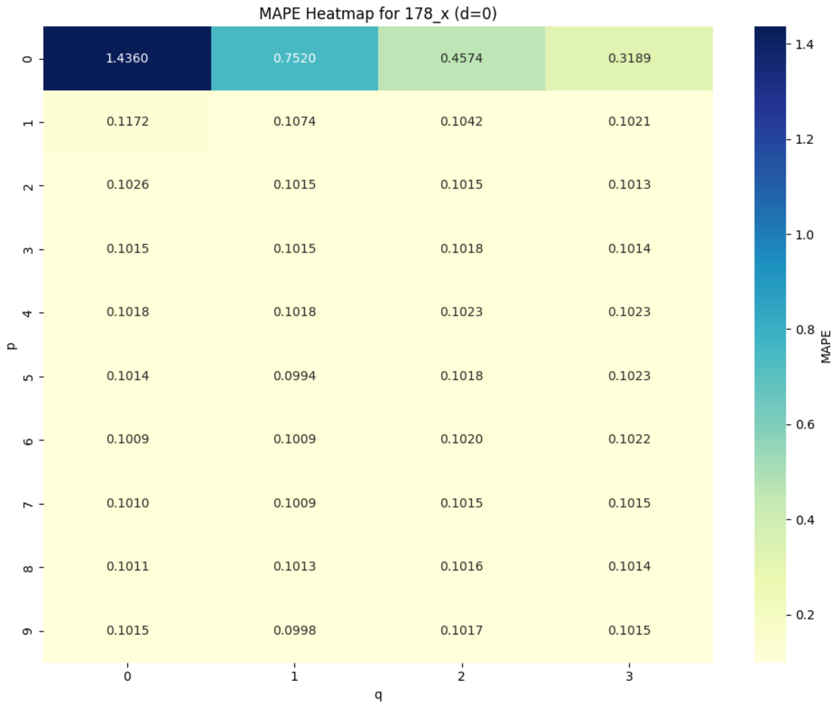

Figure 2. MAPE Heatmap for the x-Coordinate of Landmark 178 (d=0)

Figure 2 displays the MAPE heatmap for the x-coordinate of landmark 178, which achieved the best result among the MAPE values obtained with the ARIMA model. With d=0, the lowest MAPE (approximately 0.0994) was obtained with the combination p=5, q=1, while the highest MAPE (1.4360) was obtained with p=0, q=0.

For the application of the SARIMA method to the 80 different time series, hyperparameter ranges were set as p (0–9), d (0–1), q (0–3), P (0–1), D (0–1), Q (0–1), and s (25), resulting in 640 combinations per series and a total of 51,200 evaluations.

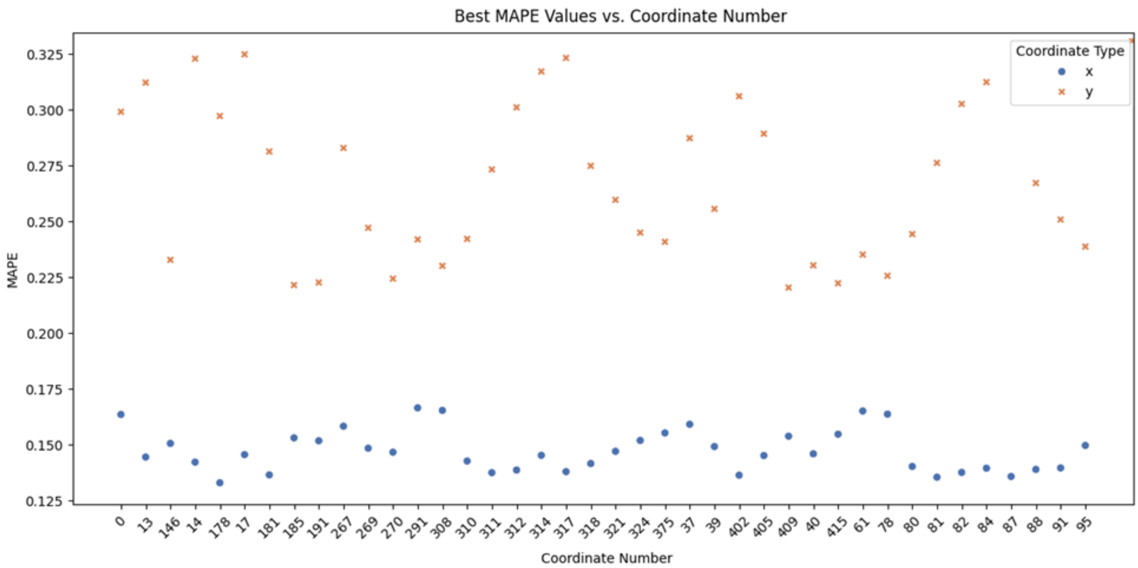

Figure 3. Best MAPE Value for Each Series

Figure 3 shows the best MAPE values for each series according to coordinate numbers. The x-coordinates (blue dots) are generally concentrated in the 0.133–0.166 MAPE range, while y-coordinates (orange crosses) are distributed in the 0.220–

0.325 range. This indicates that, similar to the ARIMA results, the coordinate type (x or y) is a determining factor in MAPE values. The lower error rates for x-coordinates suggest that these series are easier to predict compared to y-coordinates.

Table 6. MAPE Statistics by Coordinate Type

Coord. Type	Min	Max	Mean	Median
x	0.13	0.17	0.15	0.15
y	0.22	0.32	0.27	0.26

Table 6 shows that for x-coordinates, MAPE statistics are min 0.13, max 0.17, mean 0.15, and median 0.15; for y-coordinates, they are min 0.22, max 0.32, mean 0.27, and median 0.26. These values indicate that y-coordinates have approximately 80% higher average error rates and are distributed over a wider range. Overall, x-coordinates exhibit more consistent and lower error rates, while y-coordinates are more variable and challenging to predict.

Table 7. Top 10% of Series with the Lowest MAPE Values

Coordinate	p value	d value	q value	P value	D value	Q value	S value	MAPE Score
178_x	1	0	3	0	0	1	25	0.1331
81_x	1	0	3	1	0	0	25	0.1356
87_x	1	0	3	0	0	0	25	0.1359
402_x	1	0	3	0	0	0	25	0.1365
181_x	1	0	3	0	0	1	25	0.1366
311_x	1	0	3	0	0	0	25	0.1376
82_x	1	0	3	0	0	0	25	0.1377
317_x	1	0	3	0	0	0	25	0.1381

* MAPE values were rounded to four decimal places to enhance numerical clarity across coordinates.

Table 7 presents the combination values for the series in the top 10% with the lowest MAPE values. It is observed that all series in the top 10% percentile consist of X series.

Table 8. Top 10% of Series with the Highest MAPE Values

Coordinate	p value	d value	q value	P value	D value	Q value	S value	MAPE Score
17_y	0	1	3	0	0	0	25	0.3248
317_y	0	1	3	0	0	0	25	0.3232
14_y	0	1	3	0	0	0	25	0.3229
87_y	0	1	3	0	0	0	25	0.3172
314_y	0	1	3	0	0	0	25	0.3172
84_y	0	1	3	0	0	0	25	0.3124
13_y	0	1	3	0	0	0	25	0.3122
402_y	0	1	3	0	0	0	25	0.3061

* MAPE values were rounded to four decimal places to enhance numerical clarity across coordinates.

Table 8 shows the series in the worst 10% of the 80 different series based on the best MAPE values obtained using the SARIMA model, along with their parameter values and MAPE scores. The dominance of y-coordinates in the highest MAPE values confirms the modeling challenges for these series. The combinations p=0 and q=3 is frequently observed, but d=1 appears to increase the error rate in some cases.

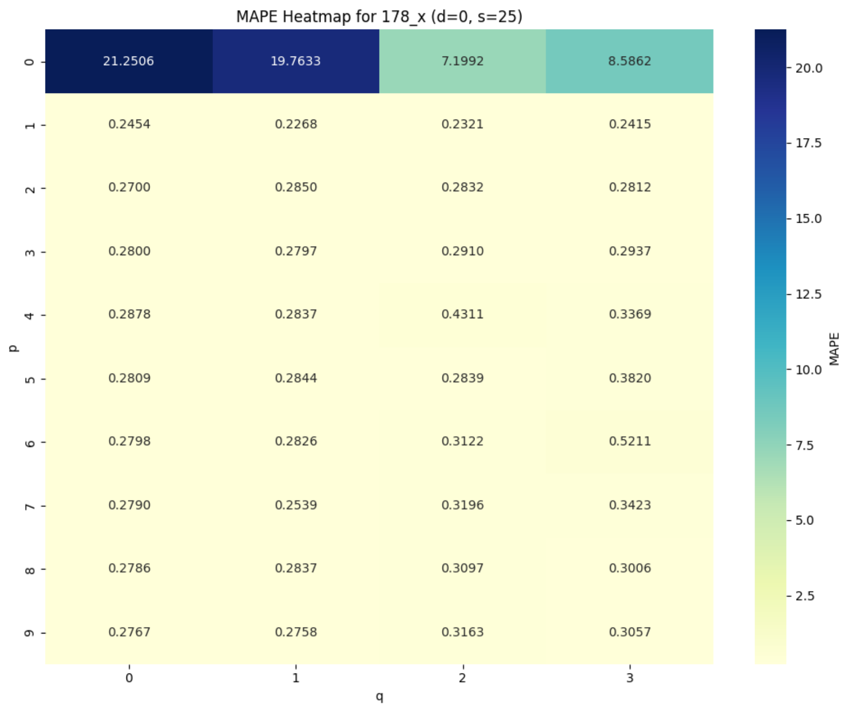

Figure 4. MAPE Heatmap for the x-Coordinate of Landmark 178 (d=0, s=25)

Figure 4 presents the MAPE heatmap for the x-coordinate of landmark 178, which achieved the best MAPE value among the 80-coordinate series when evaluated with the SARIMA method. With d=0 and s=25, the lowest MAPE (approximately 0.0994) was obtained with p=5, q=1, while the highest MAPE (1.4360) was obtained with p=0, q=0. With d=0 fixed, the effect of p and q values on MAPE is clearly demonstrated.

The most successful SARIMA parameter combinations and their frequency values are shown in Table 9. The prevalence of d=0 and q=3 combinations suggests that differencing is generally unnecessary, and a high moving average component is effective. The concentration of seasonal parameters (P, Q) at low values may indicate a limited seasonality effect.

Table 9. Top 5 Most Successful SARIMA Parameter Combinations

p value	d value	q value	P value	D value	Q value	S value	Freq.
0	1	3	0	0	0	25	37
1	0	3	0	0	0	25	27
0	1	3	0	0	1	25	5
0	1	3	1	0	0	25	4
1	0	3	0	0	1	25	3

Table 1-A (see appendix) lists the best and worst MAPE values obtained with both ARIMA and SARIMA models for each coordinate, along with the parameter combinations used to achieve these values. Generally, the best ARIMA combinations, typically 5, 0, 1 or similar parameter settings, yield MAPE values in the 0.09–0.13 range, while the best SARIMA combinations, mostly 1, 0, 3, 0, 0, 0, 25 or 1, 0, 3, 0, 0, 1, 25 produce MAPE values in the 0.13–0.32 range. Additionally, higher MAPE values are generally observed for y-coordinates. Among the worst-performing models, certain SARIMA combinations (e.g., 6, 1, 3, 0, 0, 1, 25) exhibit extremely high error rates (MAPE values exceeding 3000).

5. Discussion and Future Works

In this study, time series data derived from x and y coordinates of 40 lip landmarks, extracted using MediaPipe Face Mesh technology, were modeled using ARIMA and SARIMA methods, with forecasting performance evaluated via MAPE values. The results indicate that x-coordinates generally exhibit lower error rates compared to y-coordinates. This suggests that horizontal (x-axis) movements are temporally more regular and predictable, while vertical (y-axis) movements display greater variability. The ARIMA model, with its simpler structure and fewer parameter requirements, produced successful results for many coordinates. Notably, parameter combinations such as p=5, d=0, q=1, with minimal differencing (d=0), yielded low MAPE values. The SARIMA model, incorporating seasonal components, resulted in a broader error range for some series, indicating limited seasonality in lip coordinate data.

For future work, incorporating multivariate time series approaches (e.g., VAR, VARMA, VARMAX) could more effectively capture dependencies and simultaneous movements among lip landmarks, potentially yielding better results. Additionally, comparing machine learning and deep learning-based forecasting models (e.g., LSTM, GRU) with traditional methods is recommended as a meaningful direction for future research.

References

Aboagye-Sarfo, P., Mai, Q., Sanfilippo, F. M., Preen, D. B., Stewart, L. M., & Fatovich, D. M. (2015). A comparison of multivariate and univariate time series approaches to modelling and forecasting emergency department demand in Western Australia. Journal of Biomedical Informatics, 57, 62-73.

Adhikari, M., Joshi, P., Shrestha, S., & Shaik, S. (2025). Vision-based driver drowsiness and distraction detection through behavioral indicators of fatigue. SoutheastCon 2025, 261–266. https://doi.org/10.1109/SoutheastCon56624.2025.10971515

Ansari, M., & Alam, M. (2024). An intelligent IoT-cloud-based air pollution forecasting model using univariate time-series analysis. Arabian Journal for Science and Engineering, 49(3), 3135–3162. https://doi.org/10.1007/s13369-023-07876-9

Aripin, & Setiawan, A. (2024). Indonesian lip-reading detection and recognition based on lip shape using face mesh and long-term recurrent convolutional network. Applied Computational Intelligence and Soft Computing, 2024(1), 6479124. https://doi.org/10.1155/2024/6479124

Aroua, A., & Abdul-Nour, G. (2015). Forecast emergency room visits–a major diagnostic categories-based approach. International Journal of Metrology and Quality Engineering, 6(2), 204.

Balaji, S., & Sujatha, D. P. (2025). Hybrid eye-tracking system for cursor control: a kalman filter and exponential moving average-based approach for robust face tracking. Research Square. https://doi.org/10.21203/rs.3.rs-6541901/v1

Box, G. E. P., Jenkins, G. M., Reinsel, G. C., & Ljung, G. M. (2015). Time series analysis: Forecasting and control. John Wiley & Sons.

Brockwell, P. J., & Davis, R. A. (2016). ARMA Models. In P. J. Brockwell & R. A. Davis, Introduction to time series and forecasting (pp. 73–96). Springer International Publishing. https://doi.org/10.1007/978-3-319-29854-2_3

Butler, M. B., Gu, H., Kenney, T., & Campbell, S. G. (2016). P017: Does a busy day predict another busy day? A time-series analysis of multi-centre emergency department volumes. CJEM, 18(S1), S83-S84.

Cadenas, E., Rivera, W., Campos-Amezcua, R., & Heard, C. (2016). Wind speed prediction using a univariate ARIMA model and a multivariate NARX model. Energies, 9(2), 109.

Casals, J., García-Hiernaux, A., & Jerez, M. (2012). From general state-space to VARMAX models. Mathematics and Computers in Simulation, 82(5), 924–936. https://doi.org/10.1016/j.matcom.2012.01.001

Ding, J., Han, L., & Chen, X. (2010). Time series AR modeling with missing observations based on the polynomial transformation. Mathematical and Computer Modelling, 51(5–6), 527–536. https://doi.org/10.1016/j.mcm.2009.11.016

Ekman, P. (2003). Emotions revealed: Recognizing faces and feelings to improve communication and emotional life.(2003). Emotions Revealed: Recognizing Faces and Feelings to Improve Communication and Emotional Life. Xvii, 267.

Elamin, N., & Fukushige, M. (2018). Modeling and forecasting hourly electricity demand by SARIMAX with interactions. Energy, 165, 257–268. https://doi.org/10.1016/j.energy.2018.09.157

Gulay, E., Sen, M., & Akgun, O. B. (2024). Forecasting electricity production from various energy sources in Türkiye: A predictive analysis of time series, deep learning, and hybrid models. Energy, 286, 129566. https://doi.org/10.1016/j.energy.2023.129566

Jakhete, S. A., & Kulkarni, N. (2024). A comprehensive survey and evaluation of Mediapipe face mesh for human emotion recognition. 2024 8th International Conference on Computing, Communication, Control and Automation (ICCUBEA), 1–8. https://doi.org/10.1109/ICCUBEA61740.2024.10775188

Jiang, W., Wu, X., Gong, Y., Yu, W., & Zhong, X. (2020). Holt–Winters smoothing enhanced by fruit fly optimization algorithm to forecast monthly electricity consumption. Energy, 193, 116779. https://doi.org/10.1016/j.energy.2019.116779

Kadri, F., Harrou, F., Chaabane, S., & Tahon, C. (2014). Time series modelling and forecasting of emergency department overcrowding. Journal of Medical Systems, 38(9), 107-127.

Kong, L., Li, G., Rafique, W., Shen, S., He, Q., Khosravi, M. R., Wang, R., & Qi, L. (2024). Time-aware missing healthcare data prediction based on ARIMA model. IEEE/ACM Transactions on Computational Biology and Bioinformatics, 21(4), 1042–1050. https://doi.org/10.1109/TCBB.2022.3205064

Kumar, L., Khedlekar, S., & Khedlekar, U. K. (2024). A comparative assessment of holt winter exponential smoothing and autoregressive integrated moving average for inventory optimization in supply chains. Supply Chain Analytics, 8, 100084. https://doi.org/10.1016/j.sca.2024.100084

Li, X., Wu, K., & Zhang, S. (2024). Landmark-in-facial-component: Towards occlusion-robust facial landmark localization. Image and Vision Computing, 151, 105289. https://doi.org/10.1016/j.imavis.2024.105289

Lu, M., & Xu, X. (2024). TRNN: An efficient time-series recurrent neural network for stock price prediction. Information Sciences, 657, 119951. https://doi.org/10.1016/j.ins.2023.119951

Lugaresi, C., Tang, J., Nash, H., McClanahan, C., Uboweja, E., Hays, M., Zhang, F., Chang, C.-L., Yong, M. G., Lee, J., Chang, W.-T., Hua, W., Georg, M., & Grundmann, M. (2019). MediaPipe: a framework for building perception pipelines (No. arXiv:1906.08172). arXiv. https://doi.org/10.48550/arXiv.1906.08172

Mai, Q., Aboagye-Sarfo, P., Sanfilippo, F. M., Preen, D. B., & Fatovich, D. M. (2015). Predicting the number of emergency department presentations in Western Australia: A population-based time series analysis. Emergency Medicine Australasia, 27(1), 16-21.

Mast, M. S. (2007). On the importance of nonverbal communication in the physician–patient interaction. Patient Education and Counseling, 67(3), 315–318.

Mete, S., Çelik, E., & Gül, M. (2022). Predicting the time of bus arrival for public transportation by time series models. Journal of Transportation and Logistics, 7(2), 541–555.

Mishra, P., Al Khatib, A. M. G., Yadav, S., Ray, S., Lama, A., Kumari, B., Sharma, D., & Yadav, R. (2024). Modeling and forecasting rainfall patterns in India: A time series analysis with XGBoost algorithm. Environmental Earth Sciences, 83(6), 163. https://doi.org/10.1007/s12665-024-11481-w

Rosychuk, R. J., Youngson, E., & Rowe, B. H. (2016). Presentations to emergency departments for COPD: A time series analysis. Canadian Respiratory Journal, 2016, 1–9. https://doi.org/10.1155/2016/1382434

Serin, F., Alisan, Y., & Kece, A. (2021). Hybrid time series forecasting methods for travel time prediction. Physica A: Statistical Mechanics and Its Applications, 579, 126134. https://doi.org/10.1016/j.physa.2021.126134

Shumway, R. H., & Stoffer, D. S. (2025). Time series analysis and its applications: With R examples. Springer Nature Switzerland. https://doi.org/10.1007/978-3-031-70584-7

Siddique, M. A. B., Mahalder, B., Haque, M. M., & Ahammad, A. K. S. (2025). Forecasting air temperature and rainfall in Mymensingh, Bangladesh with ARIMA: Implications for aquaculture management. Egyptian Journal of Aquatic Research, S1687428525000251. https://doi.org/10.1016/j.ejar.2025.02.009

Sui, M., Zhang, C., Zhou, L., Liao, S., & Wei, C. (2024). An ensemble approach to stock price prediction using deep learning and time series models. 2024 IEEE 6th International Conference on Power, Intelligent Computing and Systems (ICPICS), 793–797. https://doi.org/10.1109/ICPICS62053.2024.10796661

Tripathi, R., Nayak, A. K., Raja, R., Shahid, M., Kumar, A., Mohanty, S., ... & Gautam, P. (2014). Forecasting rice productivity and production of Odisha, India, using autoregressive integrated moving average models. Advances in Agriculture, 2014.

Tsay, R. S. (2005). Analysis of Financial Time Series. John Wiley & Sons.

Tsay, R. S. (2013). Multivariate time series analysis: With R and financial applications. John Wiley & Sons.

Wahyudi, A. J., & Febriani, F. (2024). Time-series forecasting of particulate organic carbon on the Sunda Shelf: Comparative performance of the SARIMA and SARIMAX models. Regional Studies in Marine Science, 80, 103863. https://doi.org/10.1016/j.rsma.2024.103863

Wei, W., Jiang, J., Liang, H., Gao, L., Liang, B., Huang, J., ... & Qin, F. (2016). Application of a combined model with autoregressive integrated moving average (ARIMA) and generalized regression neural network (GRNN) in forecasting hepatitis incidence in Heng county, China. PloS one, 11(6), e0156768.

Wold, H. (1938). A study in the analysis of stationary time series [PhD Thesis, Almqvist & Wiksell]. https://www.diva-portal.org/smash/record.jsf?pid=diva2:492042

Xu, Q., Tsui, K. L., Jiang, W., & Guo, H. (2016). A hybrid approach for forecasting patient visits in emergency department. Quality and Reliability Engineering International, 32(8), 2751-2759.

Yucesan, M., Gul, M., & Celik, E. (2018). Performance comparison between ARIMAX, ANN and ARIMAX-ANN hybridization in sales forecasting for furniture industry. Drvna industrija: Znanstveni časopis za pitanja drvne tehnologije, 69(4), 357-370.

Yule, G. U. (1926). Why do we sometimes get nonsense-correlations between time-series?–A study in sampling and the nature of time-series. Journal of the Royal Statistical Society, 89(1), 1–63.

Yuan, C., Liu, S., & Fang, Z. (2016). Comparison of China's primary energy consumption forecasting by using ARIMA (the autoregressive integrated moving average) model and GM (1, 1) model. Energy, 100, 384-390.

Zhang, G., Zhang, X., & Feng, H. (2016). Forecasting financial time series using a methodology based on autoregressive integrated moving average and Taylor expansion. Expert Systems, 33(5), 501-516.

Zhang, W., Zhang, X., & Tang, Y. (2023). Facial expression recognition based on improved residual network. IET Image Processing, 17(7), 2005–2014. Scopus. https://doi.org/10.1049/ipr2.12743

Zhang, X., Yu, Y., Xiong, F., & Luo, L. (2020). Prediction of daily blood sampling room visits based on ARIMA and SES model. Computational and Mathematical Methods in Medicine, 2020(1), 1720134. https://doi.org/10.1155/2020/1720134

Zivot, E., & Wang, J. (Eds.). (2006). Vector autoregressive models for multivariate time series. In Modeling Financial Time Series with S-PLUS® (pp. 385–429). Springer. https://doi.org/10.1007/978-0-387-32348-0_11

APPENDIX

Table 1-A. Best and worst MAPE values obtained with ARIMA and SARIMA methods

Coord.	ARIMA			SARIMA			
	BEST		WORST	BEST		WORST	
	(p, d, q)	MAPE	MAPE	(p, d, q, P, D, Q, s)	MAPE	(p, d, q, P, D, Q, s)	MAPE
178_x	5,0,1	0.09937608	1.435977992	1,0,3,0,0,1,25	0.133050513	6,1,3,0,0,1,25	3133.920292
81_x	5,0,1	0.10168164	1.447421532	1,0,3,1,0,0,25	0.135553991	0,0,0,0,0,0,25	100
87_x	5,0,1	0.10237386	1.266574391	1,0,3,0,0,0,25	0.135892189	0,0,0,0,0,0,25	100
402_x	5,0,3	0.10296468	0.828397457	1,0,3,0,0,0,25	0.136452465	6,1,3,0,1,0,25	161.8177657
181_x	9,0,1	0.10321259	1.528204297	1,0,3,0,0,1,25	0.136598705	0,0,0,0,0,0,25	100
311_x	3,0,2	0.10375558	0.829421795	1,0,3,0,0,0,25	0.137593851	0,0,0,0,0,0,25	100
82_x	8,0,3	0.10522601	1.270162108	1,0,3,0,0,0,25	0.137692494	6,1,3,0,1,0,25	331.1700564
317_x	6,0,3	0.10511561	0.923345096	1,0,3,0,0,0,25	0.138056544	6,1,3,0,1,0,25	138.279693
312_x	3,0,2	0.10599842	0.921313308	1,0,3,0,0,0,25	0.138771163	0,0,0,0,0,0,25	100
88_x	5,0,1	0.10497560	1.592677386	0,1,3,1,0,0,25	0.139040264	6,0,3,0,1,0,25	359.5971969
84_x	5,0,1	0.10545934	1.315978034	1,0,3,0,0,0,25	0.139583	0,0,0,0,0,0,25	100
91_x	5,0,3	0.10558966	1.711664151	1,0,3,0,0,0,25	0.139723399	4,0,2,1,1,0,25	18412.73995
80_x	6,0,1	0.10584419	1.605907296	1,0,3,1,0,0,25	0.140368225	7,1,3,0,1,0,25	1007.48025
318_x	9,0,2	0.10823836	0.787790034	1,0,3,0,0,0,25	0.141668595	0,0,0,0,0,0,25	100
14_x	8,0,3	0.11058498	1.087601349	1,0,3,0,0,0,25	0.142316379	6,1,3,0,1,0,25	194.285881
310_x	9,0,2	0.10953666	0.792216458	1,0,3,0,0,0,25	0.142806091	0,0,0,0,0,0,25	100
13_x	8,0,3	0.11231879	1.089366615	1,0,3,0,0,0,25	0.144568805	4,1,2,1,1,1,25	3136.260776
405_x	3,0,2	0.11209947	0.781406271	0,1,3,0,0,1,25	0.145260372	6,1,3,0,1,0,25	193.120676
314_x	6,0,3	0.11210699	0.896873503	1,0,3,0,0,1,25	0.145364045	6,1,3,0,1,0,25	863.2600201
17_x	5,0,1	0.11146452	1.092059035	1,0,3,0,0,0,25	0.145661558	6,1,3,0,1,0,25	669.6962154
40_x	5,0,1	0.11214378	1.738231615	0,1,3,1,0,0,25	0.146025867	0,0,0,0,0,0,25	100
270_x	8,0,2	0.11321370	0.747115433	1,0,3,0,0,0,25	0.146750405	0,0,0,0,0,0,25	100
321_x	7,0,2	0.11395582	0.739733634	0,1,3,0,0,1,25	0.14715464	0,0,0,0,0,0,25	100
269_x	3,0,2	0.11591097	0.785626852	1,0,3,0,0,0,25	0.148525467	0,0,0,0,0,0,25	100
39_x	6,0,1	0.11595688	1.572304405	1,0,3,0,0,0,25	0.149286127	0,0,0,0,0,0,25	100
95_x	7,0,1	0.11527360	1.720214371	0,1,3,0,0,0,25	0.149770269	0,0,0,0,0,0,25	100
146_x	4,0,2	0.11580781	1.852531197	1,0,3,0,0,0,25	0.150677859	0,0,0,0,0,0,25	100
191_x	3,0,3	0.11677169	1.735104706	0,1,3,0,0,0,25	0.151879802	0,0,0,0,0,0,25	100
324_x	3,0,3	0.11807483	0.781246805	1,0,3,0,0,0,25	0.151995233	0,0,0,0,0,0,25	100
185_x	3,0,2	0.11825533	1.866160322	0,1,3,1,0,0,25	0.153164012	6,0,3,1,0,1,25	19807.02369
409_x	3,0,3	0.12004112	0.757987122	1,0,3,0,0,0,25	0.15392803	4,0,2,1,1,1,25	170.2169865
415_x	6,0,3	0.12085731	0.78717809	1,0,3,0,0,0,25	0.154813162	4,0,2,0,1,0,25	8528.834526
375_x	7,0,3	0.12099382	0.759801628	0,1,3,0,0,0,25	0.155368895	4,0,2,0,1,0,25	321.3556024
267_x	3,0,2	0.12671326	0.913918311	1,0,3,0,0,0,25	0.158385372	0,0,0,0,0,0,25	100
37_x	6,0,1	0.12614272	1.342226212	1,0,3,0,0,0,25	0.159250053	0,0,0,0,0,0,25	100
0_x	6,0,1	0.13160650	1.113006584	1,0,3,0,0,0,25	0.163629547	0,0,0,0,0,0,25	100
78_x	8,0,2	0.12947171	1.887034148	1,0,3,0,0,0,25	0.163796981	0,0,0,0,0,0,25	100
61_x	4,0,2	0.13052547	1.978311226	1,0,3,0,0,0,25	0.165201677	6,0,3,1,0,1,25	166.0745253
308_x	6,0,3	0.13079112	0.800457802	1,0,3,0,0,0,25	0.165458509	0,0,0,0,0,0,25	100
291_x	3,0,3	0.13185803	0.805768958	1,0,3,0,0,0,25	0.166597358	0,0,0,0,0,0,25	100

409_y	4,0,3	0.19317847	10.79446741	0,1,3,0,0,0,25	0.220444474	4,0,2,0,1,0,25	1334.940218
185_y	7,0,3	0.19516749	10.82031819	0,1,3,0,0,0,25	0.221582356	0,0,0,0,0,0,25	100
415_y	4,0,3	0.19530656	10.84401865	0,1,3,0,0,0,25	0.222381734	0,0,0,0,0,0,25	100
191_y	9,0,2	0.19591937	10.86357107	0,1,3,0,0,0,25	0.222718994	6,1,3,1,0,1,25	185.307472
270_y	6,0,2	0.19766462	10.89146523	0,1,3,0,0,0,25	0.224439292	4,1,2,0,1,0,25	137.2688519
78_y	6,0,2	0.19911389	10.77444918	0,1,3,0,0,0,25	0.225715871	6,1,3,0,1,0,25	179.4914227
308_y	4,0,3	0.20350221	10.74694029	0,1,3,0,0,0,25	0.230164229	4,0,2,0,1,0,25	386.3229999
40_y	4,0,2	0.20391242	10.90726028	0,1,3,0,0,0,25	0.230396475	0,0,0,0,0,0,25	100
146_y	6,0,1	0.20665702	10.79970753	0,1,3,0,0,0,25	0.232837765	6,1,3,0,1,0,25	189.7121921
61_y	9,0,2	0.20864385	10.7357768	0,1,3,0,0,0,25	0.235220248	0,0,0,0,0,0,25	100
95_y	5,0,1	0.21264610	10.82086875	0,1,3,0,0,1,25	0.23879431	6,1,3,0,1,0,25	288.5158727
375_y	8,0,2	0.21452793	10.79135543	0,1,3,0,0,0,25	0.240945359	6,0,3,0,0,1,25	2740891.654
291_y	7,0,0	0.21520494	10.70296935	0,1,3,0,0,0,25	0.242001198	4,0,2,0,1,1,25	9308.670746
310_y	9,0,3	0.21547824	10.93042232	0,1,3,0,0,0,25	0.242220283	0,0,0,0,0,0,25	100
80_y	4,0,2	0.21826290	10.94321673	0,1,3,0,0,0,25	0.244380664	4,1,2,0,0,1,25	1238.126899
324_y	4,0,3	0.21878916	10.81026512	0,1,3,0,0,0,25	0.245031666	0,0,0,0,0,0,25	100
269_y	7,0,2	0.22037003	10.98728604	0,1,3,0,0,0,25	0.247175417	0,0,0,0,0,0,25	100
91_y	6,0,1	0.22436393	10.87953525	0,1,3,0,0,0,25	0.250905597	0,0,0,0,0,0,25	100
39_y	7,0,2	0.22912624	10.99522356	0,1,3,0,0,0,25	0.255641984	6,1,3,0,0,0,25	124.8762493
321_y	5,0,0	0.23368296	10.8963746	0,1,3,0,0,0,25	0.259719968	0,0,0,0,0,0,25	100
88_y	8,0,3	0.24118974	10.86410158	0,1,3,0,0,0,25	0.267244044	0,0,0,0,0,0,25	100
311_y	9,0,3	0.24671998	11.01742902	0,1,3,0,0,0,25	0.273314605	0,0,0,0,0,0,25	100
318_y	6,0,2	0.24908672	10.86429984	0,1,3,0,0,0,25	0.274936472	0,0,0,0,0,0,25	100
81_y	4,0,2	0.25027510	11.02458964	0,1,3,0,0,0,25	0.276241699	0,0,0,0,0,0,25	100
181_y	7,0,2	0.25539508	10.97539704	0,1,3,0,0,0,25	0.281352583	6,0,3,1,0,1,25	5099.08556
267_y	7,0,2	0.25660685	11.06260426	0,1,3,0,0,1,25	0.282948285	0,0,0,0,0,0,25	100
37_y	8,0,3	0.26097292	11.06809729	0,1,3,0,0,1,25	0.287303265	0,0,0,0,0,0,25	100
405_y	9,0,1	0.26409151	11.00209626	0,1,3,0,0,0,25	0.289306693	0,0,0,0,0,0,25	100
178_y	8,0,3	0.27193200	10.91805419	0,1,3,0,0,0,25	0.297232966	0,0,0,0,0,0,25	100
0_y	8,0,1	0.27273381	11.1160408	0,1,3,1,0,0,25	0.299110378	0,0,0,0,0,0,25	100
312_y	9,0,1	0.27399102	11.08319996	1,1,3,0,0,1,25	0.301104343	0,0,0,0,0,0,25	100
82_y	4,0,2	0.27683224	11.08541415	1,1,3,0,0,1,25	0.302656093	0,0,0,0,0,0,25	100
402_y	2,0,3	0.28080079	10.92425628	0,1,3,0,0,0,25	0.30609919	0,0,0,0,0,0,25	100
13_y	9,0,1	0.28511938	11.11326614	0,1,3,0,0,0,25	0.31219073	0,0,0,0,0,0,25	100
84_y	7,0,2	0.28706051	11.04852261	0,1,3,0,0,0,25	0.312403903	6,0,3,0,0,1,25	121349.6688
314_y	2,0,3	0.29171824	11.06421396	0,1,3,0,0,0,25	0.317171768	0,0,0,0,0,0,25	100
87_y	1,0,3	0.29252835	10.96507303	0,1,3,0,0,0,25	0.317228345	6,1,3,1,0,1,25	140.527565
14_y	1,0,3	0.29830442	10.99049135	0,1,3,0,0,0,25	0.322901189	0,0,0,0,0,0,25	100
317_y	1,0,3	0.29866457	10.9702455	0,1,3,0,0,0,25	0.323231939	0,0,0,0,0,0,25	100
17_y	7,0,2	0.30015594	11.08009806	0,1,3,0,0,0,25	0.324837695	6,0,3,0,0,1,25	951.9562228